Estimates of Surface and Mass Erosion Following the 2016 Emerald Wildfire

Final Report to the Lake Tahoe West Shore Restoration Project

William Elliot[A,F], Longxi Cao [B], Jonathan W. Long [C], Mariana Dobre [D], Roger Lew [D], Mary Ellen Miller [E]

In Support of the Tahoe West Shore Restoration Project

[A]USDA Forest Service, Rocky Mountain Research Station, Moscow, ID 83843

[B]State Key Laboratory of Soil and Sustainable Agriculture, Institute of Soil Science, Chinese Academy of Sciences, Nanjing 210008, PR China

[C]USDA Forest Service, Pacific Northwest Research Station, Davis, CA 95616

[D] University of Idaho, Moscow, ID 83843

[E] Michigan Technological Research Institute, Ann Arbor, MI

[F]Corresponding author E-mail: welliot@fs.fed.us

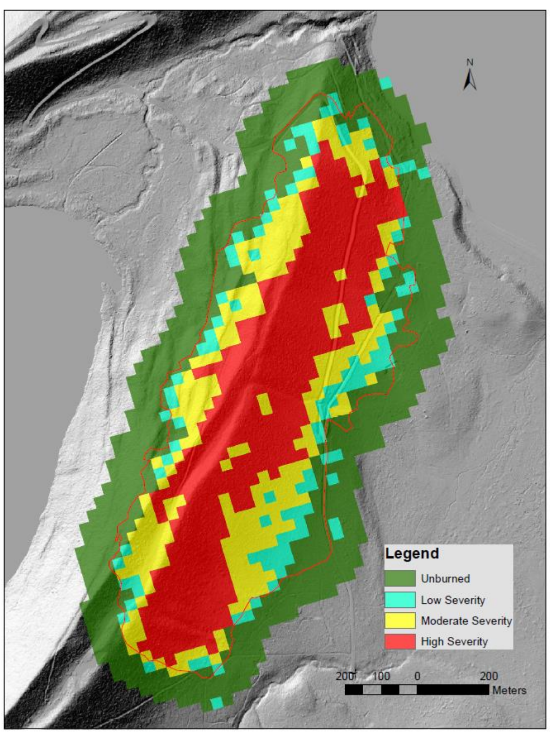

October, 2018

Soil Burn Severity Map and underlying high resolution Digital Elevation Model of 2016 Emerald Fire on the southwest shore of Lake Tahoe, CA.

Summary:

In 2016, the Emerald Fire burned 70 ha (173 acres) near the southwest corner of Lake Tahoe on the ridge between Cascade Lake and Tallac Creek. The occurrence of this fire in an area with two roads and a LIDAR elevation data set provided an opportunity to evaluate the impacts of roads on post wildfire erosion, and to test other postfire erosion modeling tools. This study evaluated road effects on soil erosion in a fire-disturbed forest with GIS technology and a soil erosion model, and the likelihood of mass failure by debris flow, translational failure and dry ravel. Results showed that roads could alter flow paths and reroute sediment transport, leading to deposition and reducing soil loss in a fire disturbed forest. WEPP-predicted sediment deposition on road surfaces and in sediment basins was similar to observed deposition. The predicted likelihood of a debris flow occurring was about 35 percent, and no debris flows have been observed. There is, however, a high likelihood of a translational landslide occurring within 4 to 6 years as the roots of the dead trees decompose. The dry ravel results suggest that there is a risk of some deposition on Highway 89 due to dry ravel until sufficient vegetation is reestablished to stabilize some of the steeper slopes.

Introduction

Following wildfire, there are six types of soil movement that may occur:

1) surface erosion associated with runoff from rainfall and snowmelt,
2) debris flows associated with increased surface runoff in upland swales,
3) translational landslides occurring several years after a fire (as tree roots that had kept the slopes stable decompose),
4) dry ravel on steep slopes when loss of live vegetation and branches releases sediment that had accumulated on the uphill side of barriers to surface sediment movement,
5) gully erosion due to increased runoff, and
6) wind erosion.

This report will address the first four forms of soil movement that have occurred, or may occur on the steep slopes following the Emerald Fire. Gully and wind erosion will not be addressed.

Soil displacement from surface erosion and mass wasting are one of the major concerns in forest management. Disturbances such as forest roads, timber harvesting, or fire increase the likelihood of forest soil movement (Elliot, 2013). Displaced sediment that is routed to forest streams or lakes can cause serious damage to the aquatic environment (McCormick et al., 2010) and impair beneficial uses of surface water resources (Elliot, 2013; Elliot et al., 2016). Roads may accumulate, deliver, or increase sediment in runoff (Gucinski et al., 2001), increasing the complexity of understanding and evaluating soil displacement and sediment transport processes in postfire forest conditions.

Fire disturbance in forests increases runoff and erosion generally due to the decrease of soil organic matter, loss of ground cover and on some soils, and the tendency for the soil to become water repellant. All of these processes leave the soil more vulnerable to water erosion (Robichaud et al., 2010). In addition, on steeper slopes, tree roots can limit mass movement of soil, but if a fire kills many of the more mature trees, and the roots die, translational mass movement can occur (Hammond et al., 1992). Surface residue from trees and shrubs can also form barriers to surface sediment movement by gravity, but if burned, may release that accumulated sediment when soils become sufficiently dry that hygroscopic forces are unable to prevent downslope movement (Fu, 2004). Soil erosion following severe wildfire can be up to three magnitudes greater than before fire (DeBano et al., 1998; Elliot, 2013) and recent deadly debris flows following wildfire underscore the dangers that need to be evaluated following wildfire in urban areas (USGS, 2018). At a watershed scale, sediment and runoff response to wildfire are often influenced by burn severity and the occurrence of hydrologic events (Robichaud, 2005; Cannon et al., 2010). An intense rainfall event following a high burn severity fire can greatly increase runoff, erosion, the initiation of debris flows and downstream sedimentation (Robichaud et al., 2000; Cannon et al., 2010, Staley et al., 2016). Topography is also a significant factor in all postfire soil erosion, with longer slopes and steeper slopes generating more sediment and increasing the likelihood of mass wasting erosion events.

Road construction may change the underlying topography and alter surface hydrology or interact with geomorphic processes (Gucinski et al., 2001; Wemple et al., 2001; Reid, 2010). Road networks linked with stream networks and may increase stream density within a watershed (Gucinski et al., 2001; Wemple et al., 1996; Croke and Mockler, 2001). Forest roads can also decrease the critical gradient for gully initiation and mass failure and reduce the distance between onsite sediment generation and downstream channels (Katz et al., 2014). The road network may also increase watershed peak flow and sediment generation rates (Jones and Grant, 1996; Thomaz et al., 2014). On the other hand, road segments can act as hydrological barriers which can change the natural flow path. Roads with upslope ditches intercept hillslope and upstream runoff that can accumulate this runoff along road surfaces before drainage through culverts, or overtopping of the accumulated runoff across the road surface (Gucinski et al., 2001; Elliot 2004; Wemple et al., 2017). Therefore flow accumulation and flow energy may be redistributed in hillslopes below road segments. This redistribution of runoff can result in altering surface soil erosion and sediment transport processes.

With the aid of GIS technology and advanced modeling methods, many researchers addressed the influence of road networks on watershed scale hydrology and sediment processes (Brooks et al., 2006; Akay et al., 2008; Araujo et al., 2014; Parsakhoo et al., 2014; Soulis et al., 2014; Grace. 2017). Most of these researchers stated that road networks would accelerate runoff accumulation processes and enhance peak flow and sediment generation in natural watersheds. However, in the case of fire-disturbed forests where large amount of sediment is generated, a road downslope of an eroding hill may change the flow route and result in unique erosion or sediment transport process. For example, a road segment may intercept high sediment concentration flow and become a site for deposition (Wemple et al., 2001; MacDonald and Coe, 2008). This implies that the road effect on sediment transport in disturbed forests may be different from that in the undisturbed conditions. The road hydrology effect is difficult to evaluate spatially as road topography cannot be precisely measured using a coarse DEM. However, the high resolution LiDAR (Light Detection and Ranging)-derived DEM can describe the topographical details for precise hydrologic analyses (Yang et al., 2014; Persendt and Gomez, 2016). The LiDAR DEM has also been used for road related flow path simulation (Sosa-Pérez and MacDonald, 2017). Thus it is possible with LIDAR data to quantify road topography more precisely and estimate how road segments influence surface runoff and sediment transport in a hilly watershed.

This study was carried out to evaluate a recent fire disturbance with road segment interactions on forest soil erosion processes in steep terrain. A GIS-based model was adopted to predict soil erosion, a USGS regression equation was used to predict the likelihood of a debris flow, and a classic soil mechanics stability equation was used to evaluate the risk of a translational landslide. A physically-based postfire dry

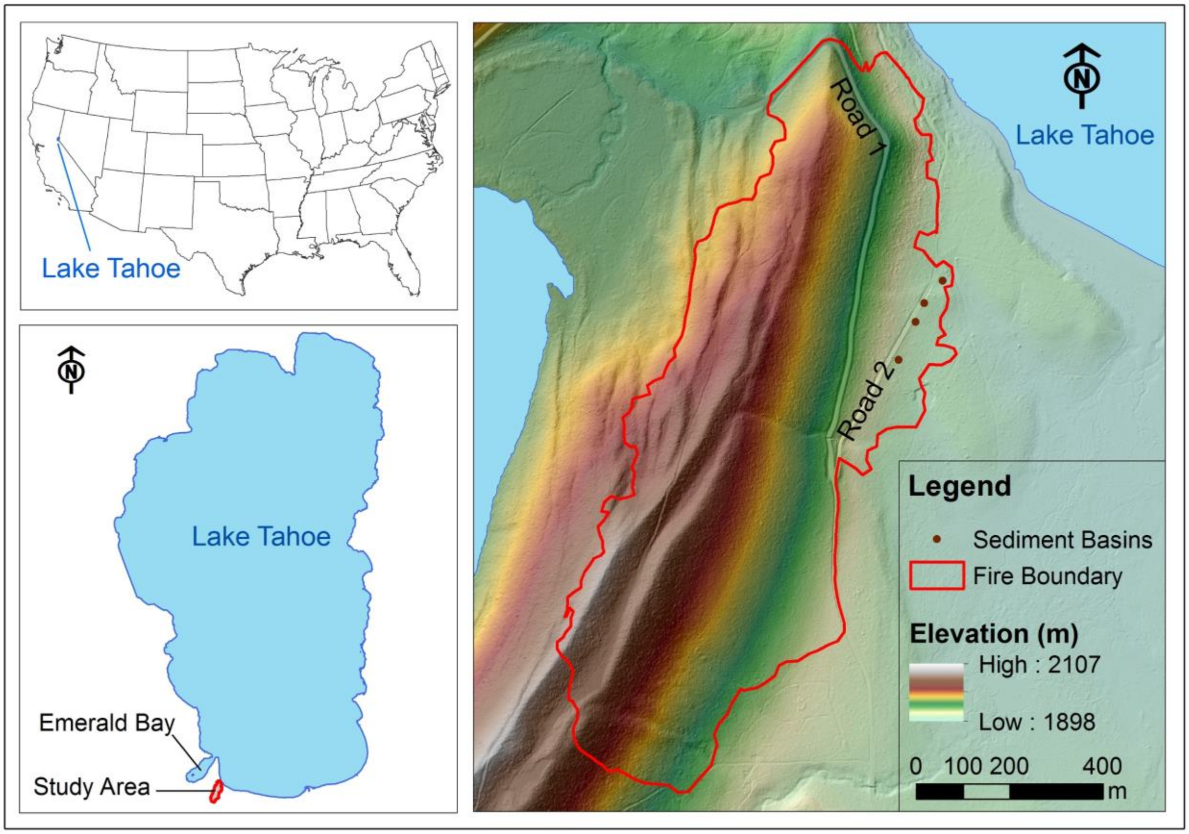

Figure 1. The location and topography of the study site represented by a LiDAR DEM.

ravel model under development by the USDA Forest Service, Rocky Mountain Research Station (RMRS) and the Michigan Technological Research Institute (MTRI) was also evaluated.

In support of the surface erosion prediction, a flow path network was delineated and the spatial distribution of soil loss was estimated based on the high resolution LiDAR DEM. A 30-m DEM was used to support the debris flow modeling, and a 2-m DEM derived from the LiDAR data to estimate slope steepness for the translational landslide analysis. The USGS 10-m DEM was used to evaluate the distribution of deposition locations associated with dry ravel. The results of this study are intended to increase our understanding of how road segments influence surface runoff and postfire sediment transport processes, determine the risk of a debris flow, determine the likelihood of a translation landslide, and identify the risk of dry ravel following the Emerald Fire in the Tahoe Basin.

Methods

Study site description

The study site was near the Emerald Bay on the southwest shore of Lake Tahoe in California, USA (Figure 1). Vegetation is comprised of mixed conifer forest with significant areas covered by meadows, riparian areas, or bare granite outcrops (Coats et al., 2008; Nevada Division of Environmental Protection, 2011). Lake Tahoe is the largest alpine lake in North American has long been renowned for its exceptional clarity.

However, erosion resulting from forest clearing and urban development over the past century and a half has degraded that clarity, leading to the establishment of a Total Maximum Daily Load for fine sediment particles, nitrogen, and phosphorus (Nevada Division of Environmental Protection, 2011). The climate is comprised of wet winters and dry summers. Influences from the Pacific Ocean and orographic effects result in extreme precipitation differences between the west and east sides of the lake, with the annual precipitation ranging from 600 mm on the eastern shore at lake level to more than 1600 mm on the western crest (PRISM Layer at http://wepp2.nkn.uidaho.edu/lt/) The basin's hydrology is dominated by snowfall accumulation and melt, especially at higher elevations, and rain-on-snow events, at lower elevations (Brooks et al., 2016).

The Emerald Fire started early in the morning of October 14, 2016. Fueled by high winds (gusting up to 89 km/h), it burned 71 ha (red boundary in Fig. 1) by the following morning, when heavy rainfall extinguished the fire (http://wildfiretoday.com/2016/10/14/200-acre-emerald-fire-at-lake-tahoe-slowed-by-rain/). Precipitation depths of 81, 56, and 114 mm were recorded at the nearby Echo Peak SnoTel Site for October 14, 15 and 16, respectively, for a total depth of 251 mm in three days. Most of the area was covered by forest before fire disturbance. Highway 89 (Road 1 in Fig. 1) and another paved road (Cascade Road) (Road 2 in Fig. 1) pass through the northeast part of the burn site. According to our field survey, road 1 is flat without ditches and road 2 is crowned with ditches. The hillslope between the ridge and road 2 is generally uniform with an average gradient of about 30 percent. The average gradient of hillslope below road 2 is about 17 percent. The channel from the largest watershed likely to generate a debris flow passed under the two roads near their intersection (Figure 1).

Following the fire, the California Department of Transport removed a large amount of sediment that was deposited on Highway 89 (Road 1) in order to keep the road open. Eldorado County had to empty four sediment basins that had overtopped on cross drains below Cascade Road (Road 2, Figure 1) and a large accumulation of sediment in an old quarry about 100 m below Road 2. The sediment was attributed to surface erosion as there was no evidence of a debris flow in the only large channel in the burned area.

Data collection and preparation

LiDAR terrain data were used to define flow paths and delineate the topography of roads in the study site for the erosion study. The LiDAR remote sensing data of Lake Tahoe were collected by Watershed Sciences, Inc. (WSI) in August 2010. The survey used two Leica ALS50 Phase II laser systems mounted in a Cessna Caravan 208B. A raster elevation data set with a resolution of 0.5 m was created based on the ground return points from the LiDAR flight (Fig. 1).

We estimated soil burn severity using the differenced Normalized Burn Ratio (dNBR) from Landsat ETM 7 images from information before and after the fire to generate a Burned Area Reflectance Classification (BARC) layer (Parsons et al., 2010). The BARC data were classified following Parsons et al., (2010) to estimate soil burn severity (Table 1).

Erosion modeling

Michigan Technological Research Institute (MTRI), together with US Forest Service and NASA, developed a rapid response tool to provide a digital elevation model, soil and land cover layers, and the linkage files necessary to run GeoWEPP (an ArcMap Wizard to the Water Erosion Prediction Project

Table 1. Distribution of estimated soil burn severity categories after the Emerald fire

Burn Severity	dNBR* range	Area (ha)	Percent (%)
Unburned	⩽ 99	9.43	13.28
Low Severity	100-269	8.25	11.62
Moderate Severity	270-659	20.65	29.08
High Severity	⩾ 660	32.67	46.01

* Differenced Normalized Burn Ratio

Watershed Version) simulations of postfire erosion[1] (Miller et al., 2016). We uploaded the BARC raster map onto the MTRI main page, and then downloaded soil and land use files formatted for GeoWEPP (Miller et al., 2015) for the study site. The LANDFIRE Existing Vegetation Type (EVT) data downloaded from the Miller et al., (2016) server were adopted as the prefire land cover. Soil and land use data were provided as 30-m resolution raster files and stored in an ASCII format, including both pre-fire and postfire conditions. The postfire soil properties modification was achieved following the instructions described by Elliot and Hall (2010). We were then able to run the WEPP model spatially under different soil and land use types describing both pre-fire and postfire conditions.

WEPP is a physically-based soil erosion model (Laflen et al., 1997), and is particularly suited to modeling the conditions common in forests (Elliot et al., 2001; Elliot, 2013). WEPP can be run either for an individual hillslope with a representative steepness and length, or as a watershed where individual hillslope runs are combined with a channel network to predict upland erosion for each hillslope and channel erosion, deposition and sediment delivery. The WEPP model operates on a daily time step, carrying out a soil water balance including evapotranspiration, lateral flow and deep seepage, and if there is precipitation or snowmelt, estimating runoff and soil detachment, transport and delivery from a hillside. If desired, the user can specify for each day the growing or senescing plants and accumulating and decomposing of vegetative litter on the ground surface (Flanagan and Nearing, 1995).

GeoWEPP is a GIS platform which allows users to import and utilize their own detailed terrain, soil and landuse information or to access publicly available spatial datasets for geospatial application of the WEPP model (Flanagan et al., 2013). The GeoWEPP model version 10.3 was adopted in the AcrGIS 10.3.1 environment for soil erosion modeling in the Emerald fire area. Topography, soil and landuse data were preprocessed before running the model to ensure the GIS projections were compatible. According to our results based on local terrain, the 0.5-m LiDAR DEM would likely generate too many flow paths, exceeding the maximum memory limitation in GeoWEPP running on a PC. Therefore the 0.5-m DEM was resampled as a 2-m DEM with the ArcMap Resample tool using the "Bilinear" method for hydrological process simulation and soil loss prediction. The 30-m resolution soil and landuse data were also resampled as 2-m raster files to be compatible with the 2-m DEM using the "Nearest" method to maintain consistent pixel values. The original downloaded soil data did not delineate the road surfaces, so the soil erodibility properties for the road pixels were revised to describe paved conditions for those cells.

The GeoWEPP GIS wizard can be run in two modes, "watershed" and "flowpath." (Flanagan et al., 2013) When running in watershed mode, GeoWEPP lumps the shallow lateral flow, surface runoff and erosion response for each 2-10 ha hillslope polygon, and then routes the runoff and sediment through the

[1] http://geodjango.mtri.org/geowepp/

stream network for each storm. The output from a watershed run is sediment loss and runoff for each hillslope and channel segment. In the flowpath mode, GeoWEPP estimates the erosion for each pixel in the DEM abstracting the erosion for that point from the distributed erosion predicted by the WEPP model. Each individual flowpath is 0.2 to 0.5 ha. The flowpath method is not intended to be used to predict sediment delivery, but the output from a GeoWEPP flowpath run will include an average erosion rate for each hillslope polygon. The "flowpaths" as defined by GeoWEPP are not the same as the flow path lengths as defined by the ArcMap Spatial Analyst for routing runoff as described later, and although the GIS steps in their derivation are similar, they are not identical (http://desktop.arcgis.com/en/arcmap/; Flanagan et al., 2013). We apologize for the two methods using similar terminology, but will do our best to minimize confusion between the two different uses of the "flowpath" term.

GeoWEPP first delineates channel networks using the TOPAZ program (Flanagan et al., 2013). A critical source area (CSA) of 0.5 ha was specified for TOPAZ to generate a channel network that linked to most of the hillslopes within the Emerald fire area. For some hillslopes that were hydrologically independent from the adjacent areas, a CSA of 0.3 ha was used to generate more detail channels to reach these slopes. GeoWEPP then builds a watershed of hillslope sub-catchments and individual flow paths that, along with channel segment topography, serve as inputs to the WEPP Watershed version. Offsite sediment yields for both pre-fire and postfire conditions in the study area were estimated based on sub-catchments (select "Watershed" as the GeoWEPP simulation method). For the postfire run, a climate file was built for the year 2016 using the observed daily temperature and precipitation data from the Echo Peak SnoTel station located 12 km south of the fire. The pre-fire erosion modeling was carried out using long-term observed data from the same station and run for 20 years to simulate the normal forest conditions. For the purpose of evaluating the effect of road segments on postfire surface flow accumulation and sediment transport, a flow path simulation was carried out and the onsite soil loss was estimated for each 2-m pixel.

Spatial and hydrological analysis methods

GIS-based spatial analysis and digital terrain analyses were adopted to explore the spatial distribution of flow paths and predicted onsite soil loss rates. The Spatial Analyst Tools distributed with AcrGIS 10.3.1 were used evaluate the effects of roads and other terrain features on flow directions, while the "flowpath" mode in GeoWEPP was used to estimate the erosion rate for each pixel. The hydrological analysis tool was adopted to calculate the upstream flow length for each pixel and delineate sub-catchment boundaries. The Buffer Wizard was applied to generate 10-m buffer belts in the downslope direction of the ridge and roads. Then the onsite soil loss rates were extracted and calculated to explore the spatial variation in the estimated soil erosion.

Debris flow modeling

The debris flow modeling was based on the Cannon et al. (2010) debris flow algorithms. The probability of a landslide occurring (*P*) following wildfire on a given landscape can be estimated by the empirical relationship:

$$P = \exp(x) / (1.0 + \exp(x)), \text{ and}$$

$$x = -0.7 + 0.03 * A\_pct - 1.6 * R + 0.06 * B\_pct + 0.07 * I + 0.2 * C - 0.4 * LL \qquad (1)$$

where,

*A_p*ct is the percentage of the basin area with gradients greater than or equal to 30%,

R is basin ruggedness (Change in basin elevation divided by the square root of the basin area (Melton, 1965)),

B_pct is the percentage of the basin area burned at high and moderate severity,

I is average storm rainfall intensity (in mm/h),

C is clay content (in %),

LL is the liquid limit of the soil.

A complementary equation from Cannon et al. (2010) to estimate the volume *V* of delivered material should a landslide occur is:

$$V = \exp(7.2 + 0.6 * \log(A) + 0.7 * B^{0.5} + 0.2\, P^{0.5} + 0.3) \qquad (2)$$

Where:

A (km^2) is the area of the basin having slopes greater than or equal to 30%,

B (km^2) is the area of the basin burned at high and moderate severity,

P (mm) is the total storm rainfall, and 0.3 is a bias correction that changes the predicted estimate from a median to a mean value (Helsel and Hirsch, 2002).

The values for the variables in equations 1 and 2 were all determined by the WEPP Cloud interface[2]. The soil burn severity map provided the boundary for the analysis (Fig. 1) and the underlying DEM was accessed to estimate *A*. The soil burn severity map and the SSURGO database were combined to determine *B*. The storm intensity *I* and precipitation depth *P* values were obtained from the NOAA Precipitation Frequency Data Server[3]. The soil clay content *C* and liquid limit *LL* were obtained from the SSURGO database.

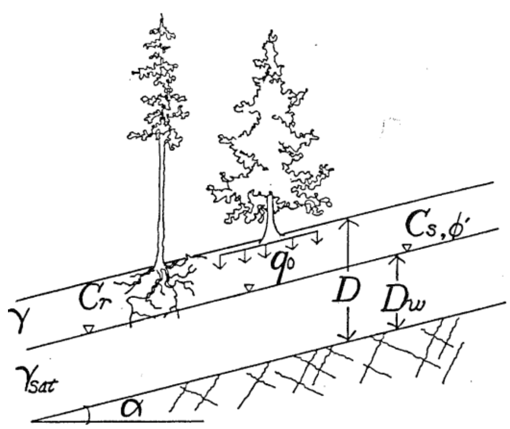

Figure 2. Dimensions and other variables associated with the infinite slope equation

[2] https://wepp1.nkn.uidaho.edu/weppcloud/

[3] https://hdsc.nws.noaa.gov/hdsc/pfds/

Translational landslide modeling

Steep slopes are prone to translational landslides when the forces driving downhill movement of soil (soil and vegetation mass) exceed the soil shear strength to offset those forces. A ratio of these two forces is used to determine a factor of safety (*FS*), where a factor of safety greater than 1 suggests a stable slope, whereas a value less than one suggests a potential failure. Figure 2 is a sketch of the variables in the infinite slope stability equation. The infinite slope equation for a forested hillslope is:

$$FS = \frac{C_r + C_S' + \cos^2(\alpha)[q_0 + \gamma(D - D_w) + (\gamma_{sat} - \gamma_w)D_w]\tan(\emptyset')}{\sin(\alpha)\cos(\alpha)[q_0 + \gamma(D - D_w) + \gamma_{sat}D_w]} \quad (3)$$

Where *FS* = factor of safety; α = slope steepness of ground surface; *D* = total soil thickness; D_w = saturated soil thickness; C_r = tree root strength expressed as cohesion (lbs ft^{-2} or N m^{-2}), q_0 = tree surcharge; C'_s = soil cohesion, ϕ' = effective soil internal angle of friction, γ_d = dry soil unit weight; γ = moist soil unity weight; γ_{sat} = saturated soil unit weight; and γ_w = water unit weight. Units can either be metric or English, but must be consistent for all variables.

Dry Ravel Modeling

The dry ravel model was developed to support Burned Area Emergency Response Teams (BAER) in California. The model is based on grid cells as potential sources or sinks of sediment moving on the ground surface. The source of this sediment is assumed to be material that has accumulated uphill of shrub stems and branches, and supported on steep slopes by plant roots. When a wildfire occurs and stems and branches are consumed, the material is free to roll on downslope if the slope is steeper than the soil's angle of repose. Released sediment is then available to move on down the hill, initiating additional sediment movement if the slope continues to be steep, or coming to rest if the slope moderates and becomes less than the angle of repose. Fu (2004) describes the modeling assumptions in detail, using a grid-based approach. MTRI has incorporated the Fu (2004) model into a GIS, and presents the results as deposition rates in cells displayed in Google Earth. Users can then evaluate if the deposition is in upland channels, and readily available for channel erosion from the next runoff event, of if the deposition is in another area of concern, like a road.

Results

Soil erosion before and after wildfire disturbance

The long-term WEPP simulation predicted that nearly 99 percent of the study area experienced an average annual erosion rate less than 0.25 Mg ha^{-1} before the fire disturbance. In the postfire condition, erosion risk increased considerably (Figure 3). Following the fire, 77.6 percent of the burned area had predicted erosion rates greater than 4 Mg ha^{-1} yr^{-1}. The percent of the area with annual erosion rates less than 0.25 Mg ha^{-1} was reduced to 18.7 percent. Table 2 shows the distribution of predicted postfire erosion rates for different burn severities. It can be seen that as burn severity increases, the area with a predicted erosion rates greater than 4 Mg ha^{-1} yr^{-1}increases, and the area with the predicted erosion rate less than 0.25 Mg ha^{-1} yr^{-1} decreases. The high burn severity and moderate severity land account for 46 percent and 29 percent respectively of the total study area. On 95 percent of the high burn severity and 81.2 percent of the moderate severity land, predicted erosion rates were greater than 4 Mg ha^{-1} yr^{-1}. The high and moderate areas accounted for 86.8 percent of the most intensive erosion class and 56.3 percent was associated with the high burn severity. The

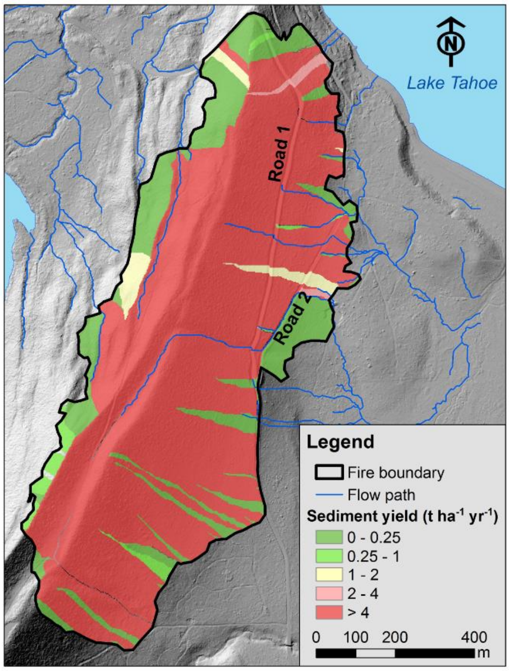

Figure 3. Distribution of estimated hillslope erosion rates after the fire disturbance (in metric tons ha^{-1} yr^{-1} or Mg ha^{-1} yr^{-1}).

low burn severity and unburned land account for 11.6 and 13.3 percent of the total study area. Only 49.8 percent of the low burn severity and 34.8 percent unburned land experienced an average annual erosion rate greater than 4 Mg ha^{-1} yr^{-1}. These lands accounted for 67.8 percent of the total area with a predicted erosion rate less than 0.25 Mg ha^{-1} yr^{-1}. The unburned land accounted for 40.6 percent of the total lowest erosion rate yield category (<0.25 Mg ha^{-1}) in the study area.

The underlying topography also influences the predicted soil erosion rates. Figure 3 shows higher erosion rates on longer hillslopes. The high erosion rate patch spread beyond the fire disturbance boundary in some cases. Figure 3 also shows that some road segments can intercept the hillslope and act as boundaries to areas of high erosion rates. The shape of some erosion patches are changed by road segments. Furthermore, in some cases, the erosion rates in the patches below a road are lower than that of the adjacent hillslope segment above the road. These results show that the road segments changed the spatial distribution of postfire erosion rates.

Table 2. Predicted postfire sediment yield under different burn severities

Sediment yield (Mg ha^{-1} yr^{-1})	Area under different burn severities (ha)[A]				
	Unburned	Low	Moderate	High	Total
0 - 0.25	4.95	3.31	2.92	1.00	12.18
0.25 - 1	0.66	0.08	0.27	0.27	1.28
1 - 2	0.43	0.52	0.47	0.26	1.68
2 - 4	0.10	0.14	0.19	0.07	0.5
> 4	3.20	4.03	16.66	30.82	54.71

[A] The total area modeled with GeoWEPP is slightly smaller than Table 1 as channel areas are not included in GeoWEPP hillslopes

Road segment effect on hydro-geomorphology characteristics

Road-related flow paths were extracted with different critical source area (CSA) values and a detailed analysis was carried out on the effects of the road topography on predicted erosion rates. ArcMap flow paths that intersected with the upslope side road edges were recognized as inflow, and outflow paths were those that intersected with road edge on the downslope side (Table 3). As the CSA was reduced, the number of flow paths increased and the average distance between flow paths decreased. It can be seen in Table 3 that the number of outflow paths is less than that of the inflow paths. This effect is especially noticeable for the smaller CSA with more dense flow paths, where a larger portion of inflow paths are intercepted by road segments and result in relatively fewer outflow paths than that of the 1000 m^2 CSA in Table 3. Road 2 which falls below road 1 showed a lower density of outflow paths with a similar inflow density when CSA was 1000 m^2. In the case of the 200 m^2 CSA, the average distance between outflow paths for road 2 is more than twice the distance than that of the road 1.

Further analyses were conducted to demonstrate road segment effect on surface hydro-geomorphology characteristics. Road segments which fall inside the burn boundary were chosen and the surrounding sub-catchments were delineated with the critical source area (CSA) of 0.5 ha (Fig. 3). The hydrological units were then overlaid with the surface topography and road segments to determine the effects of roads on sub-catchment delineation. All sub-catchments in Fig. 3 are connected to roads and can be classified as five types according to the spatial position with road segments (Table 4). There are 17 sub-catchments which pass through road segments and finally reach the fire boundary. These hydrologic units account for 47% of the total area and small channel diversions were predicted when the subcatchment cannels intersected with road segments. On the other hand, 43% of the sub-catchments which started from ridge were intercepted and ended by the two road segments. In addition, 9 new hydrologic units were formed downslope of road segments. In spite of the shorter length, road 2 with its ditches is more efficient

Table 3. Description of road related flow paths with different CSA values

Type of flow paths	Flow path CSA = 1000 m^2		Flow path CSA = 400 m^2		Flow path CSA = 200 m^2	
	Number	DBF (m) [A]	Number	DBF (m) [A]	Number	DBF (m) [A]
Flow into road 1	44	20.91	88	10.45	124	7.42
Flow out of road 1	41	22.44	58	15.86	72	12.78
Flow into road 2	23	20.52	35	13.49	41	11.51
Flow out of road 2	15	31.47	17	27.76	18	26.22

[A] DBF stand for the average distance between flow paths which was calculated as road length divided by the flow path number.

Table 4. Description of road related sub-catchments

Type of sub-catchments	Number	Area (ha)	Area ratio (%)
From ridge and reach boundary	17	14.85	46.96
From ridge and ended by road 1	1	1.31	4.15
From ridge and ended by road 2	10	12.26	38.77
From road 1 and reach boundary	3	0.90	2.84
From road 2 and reach boundary	6	2.30	7.28

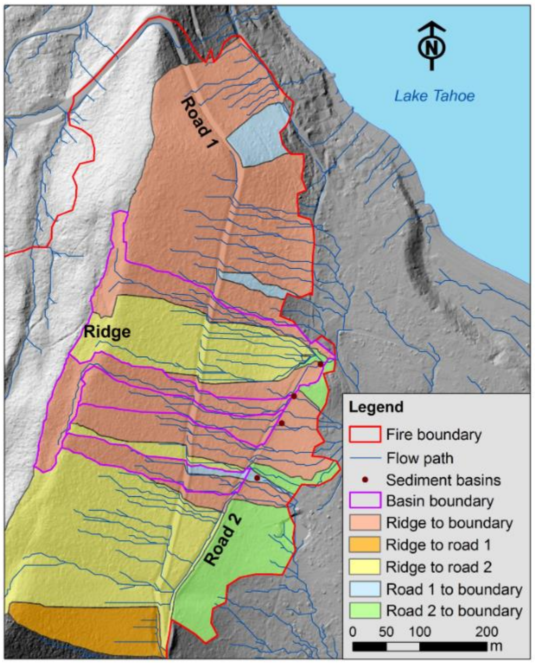

Fig. 4. Road related sub-catchment delineation

than road 1 in intercepting upstream sub-catchments and generating new ones. It also should be noted that there are 4 sediment basins installed to trap road sediment below road 2. Some of the sub-catchments are interrupted and recombined as contributing areas for the sediment basins (Fig. 4).

The effect of road segments on surface hydrological process was further studied in the context of flow length. Upstream flow length was overlaid with road segments (Fig. 5). The 2-m LiDAR DEM which can show the terrain in great detail resulted in large number of flow initial points (flow length = 0, blue

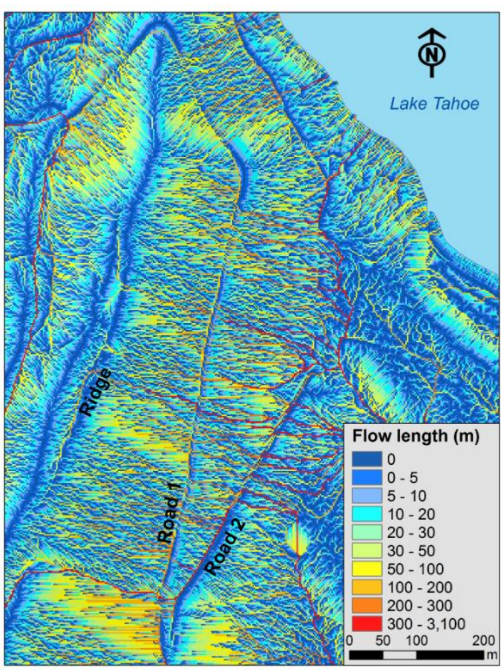

Fig. 5. Flow length as influenced by road segments

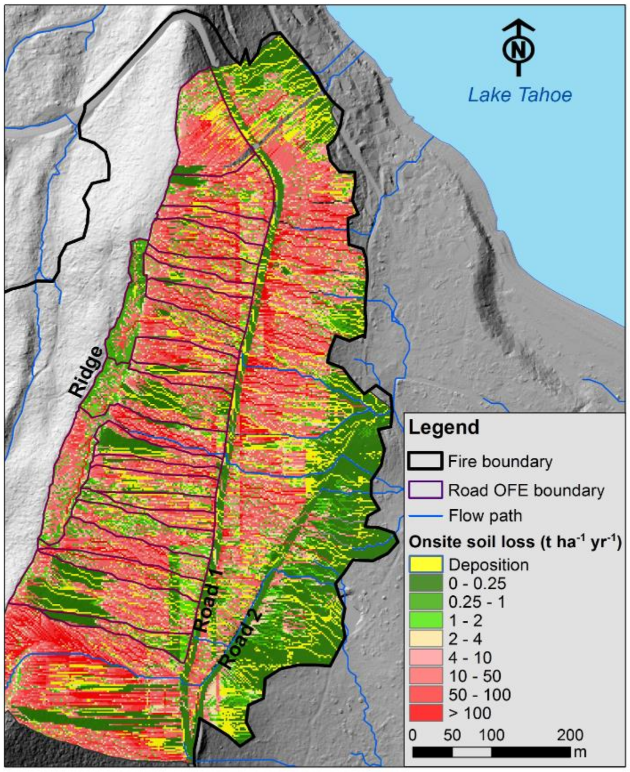

Fig. 6. Simulated onsite soil loss for the postfire condition using the GeoWEPP Flowpath Model

color) along the hillslope. It can be seen that road segments can stop the upstream flow length accumulation and start new flow path below roads. In the case of road 2, most of the upstream flow paths were intercepted and the new flow length below is shorter than that above road segment. The intercepted flow paths along road 2 accumulated for more than 300 m length (red color) and finally drained out through culverts. For road 1 which has no ditches or culverts for most of its length, some of the upstream flow paths were intercepted and stopped. However, it also can be seen that many upstream flow paths pass over road 1 after a slightly direction change. The flow then continues to accumulate length in the downslope direction.

Road segment effect on soil loss prediction

To evaluate the effect of road segments on soil loss prediction, GeoWEPP was run in the "Flowpath" mode simulated onsite soil loss near road segments under the postfire conditions. The results of the Flowpath run are presented in Figure 6. It can be seen that the paved road surface showed very low soil loss and can be distinguished from other areas easily. In some locations, deposition (yellow pixels) was predicted to occur on the road surface when a flow path reached a road segment. Detailed deposition on the surface of road 1 was simulated by running 22 different hillslope profiles that intersected with Road 1 in WEPP Windows. From these runs, the average annual sediment deposition along the road segment within the fire was calculated as 40.4 kg m^{-2}, or a sediment deposition depth averaging 4 cm on the Road 1 surface.

To evaluate the surface hydrology unit effect on soil loss due to road influence, the onsite soil loss was classified into 6 categories and overlaid with sub-catchments. Table 5 shows that sub-catchments that originated from the ridge resulted in a larger fraction of the high soil loss category (greater than 4 Mg ha^{-1} yr^{-1}) than the sub-catchments below road. The average soil loss rate also showed that ridge-originated sub-catchments had the greatest onsite soil loss. Similarly, the sub-catchments below roads showed relatively

Table 5. Onsite soil loss rate in different types of sub-catchments

Soil loss rate ($Mg\ ha^{-1}\ yr^{-1}$)	Ridge to boundary		Ridge to R1		Ridge to R2		R1 to boundary		R2 to boundary	
	Area (ha)	Ratio (%)	Area (ha)	Ratio (%)	Area (ha)	Ratio (%)	Area (ha)	Ratio (%)	Area (ha)	Ratio (%)
Deposition	1.48	10.25	0.15	11.39	0.81	7.47	0.15	16.79	0.39	17.87
0-0.25	2.54	17.55	0.55	41.96	0.96	8.84	0.14	15.05	1.21	55.89
0.25-1.0	0.85	5.85	0.03	2.09	0.68	6.31	0.04	4.62	0.15	6.84
1.0-2.0	0.79	5.48	0.04	3.01	0.59	5.44	0.04	4.13	0.09	4.28
2.0-4.0	1.04	7.18	0.05	3.5	0.76	6.96	0.07	7.82	0.14	6.27
> 4.0	7.75	53.67	0.5	38.06	7.06	64.98	0.46	51.6	0.19	8.85
Ave. soil loss ($Mg\ ha^{-1}\ yr^{-1}$)	25.33		28.03		36.38		16.05		-0.06	

more deposition and much lower average soil loss rates than those above roads. For sub-catchments below road 2, the average predicted onsite soil loss was negative, indicating that deposition was the dominate process.

To explore soil erosion variation with terrain positions in more detail, the onsite soil loss rate for different distances from ridge and road segments was measured by buffer analysis. There are 13 buffer belts below the ridge and 10 belts below each road segment. The predicted onsite soil loss rate was extracted by each 10-m-width belt, and then the average value was calculated and plotted with distance (Fig. 7). It can be seen that the average onsite soil loss rate below ridge increased exponentially with the downslope distance. On the other hand, the average soil loss rates below both road 1 and road 2 showed a logarithmically declining trend with the downslope distance. The first 10 m buffer belt below roads showed remarkably higher soil loss rate compared to the following belts. It also can be seen that the average onsite soil loss within the first 10 m belt below road 1 is close to that of the last belt below the ridge. Similarly, the average onsite soil loss rate within the first belt below road 2 was similar to the last belt below road 1. When flow path goes beyond 50 m downslope of the road 2, average soil loss rates become negative, which

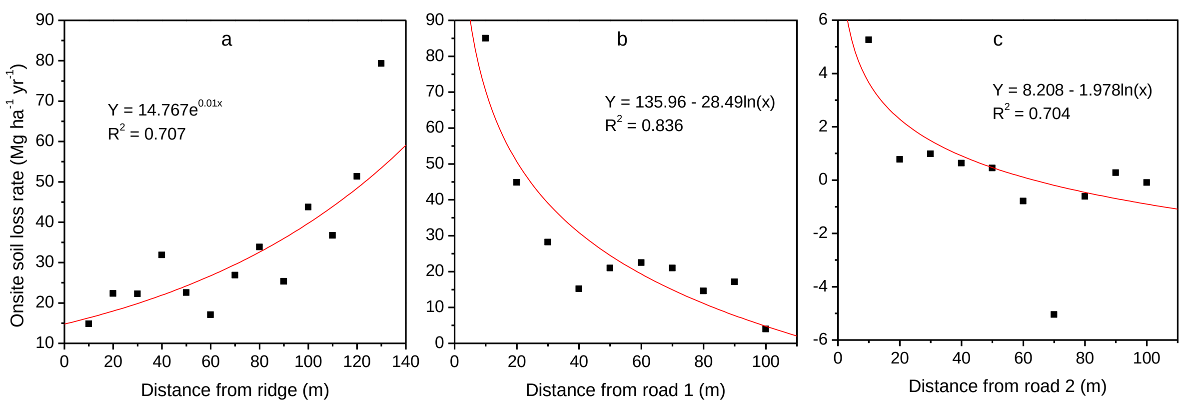

Fig. 7. The relationship between average onsite soil loss rate and downslope for a) distance from the ridgetop, b) downhill from road 1 and c) downhill from road 2.

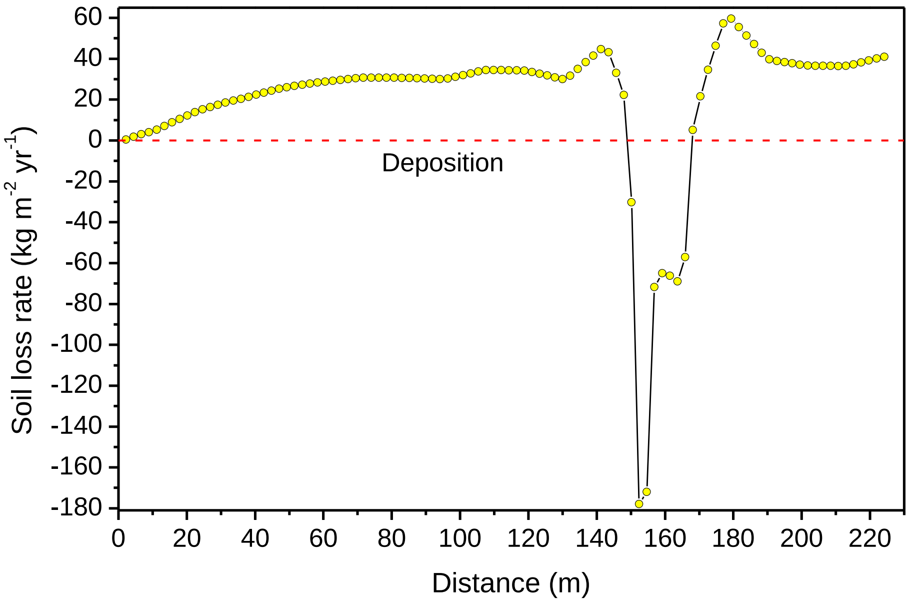

Fig. 8. Predicted soil loss rate along a hillslope passing over a road segment. A negative "soil loss" is the way the WEPP output describes deposition

means that these are sites of deposition. This is consistent with the earlier results that measured erosion by sub-catchment and observations in the field. It should be noted that the average onsite soil loss rate 70 m below road 2 (Fig. 7.c) showed an abnormally low value due to the high deposition rates predicted 70 m below the intersection of roads 1 and 2 (Fig. 6) and low to no erosion rates predicted elsewhere 70 m below road 2. This low value was not included when developing the regression equation shown on the graph.

From the GeoWEPP outputs, a typical hillslope that passed through road 1 with the same slope profile and identical soil properties was selected and run on its own in WEPP Windows to generate a typical soil loss graph along the hillslope profile (Fig. 8). Figure 8 shows that the erosion rate generally increases as the slope length stretches from 0 to 140 m due to runoff accumulation. When reaching the road segment, the erosion rate dramatically decreased and deposition occurred on the road surface section. As runoff leaves the road and continues flowing downslope, soil loss rate increases sharply within a short distance below road segment, likely due to the steep fillslope and clearer water. The loss reaches a maximum value for the profile, and then moderates as increased runoff is offset by a decreasing slope steepness below the road.

Comparing Modeling Results with Initial ERMiT Predictions by the BAER Team

The original postfire erosion analysis was carried out by a Forest Service Burned Area Emergency Response (BAER) specialist using the ERMiT tool (Robichaud et al., 2007) to quickly estimate upland erosion for the Emerald Fire (Table 6; Young, 2016). Young (2016) followed recommended methods and only presented potential erosion from 2-, 5- and 10-year events, as the probability of a more severe event was unlikely. The three recorded precipitation events that occurred immediately following the wildfire (81, 56, and 114 mm) were similar to the 5 to 10-year return period range of the ERMiT predictions for single

Table 6. Single event runoff, precipitation, erosion rates and sediment delivery estimated by ERMiT for the postfire BAER analysis (Young, 2016).

	ERMiT Hillslope Estimates		
	2-year event	5-year event	10-year event
Runoff (mm)	17.02	29.21	37.34
Precip (mm)	44.20	90.68	35.31[a]
Ave. Erosion Rate (Mg ha^{-1})	0.22	6.15	14.76
Max. Erosion Rate (Mg ha^{-1})	0.85	29.83	52.51
Erosion Production (Mg)	36.18	257.45	538.0

[a] Runoff is greater than precipitation because of snowmelt on this predicted March runoff event

storms (Table 6), if a rainfall event had been the cause of ERMiT's 10-y runoff event rather than rain-on-snow. Thus Young's (2016) selection of events was close to what actually occurred. We estimated a spatially averaged erosion rate of 16-25 Mg ha^{-1}, depending on hillslope profile for the three observed storms. The ERMiT predictions for these three storms would be approximately one 2-y event (0.22 Mg ha^{-1}), one 5-y event (6.15 Mg ha^{-1}) and one 10-y event (14.76 Mg ha^{-1}) for a total of about 21 Mg ha^{-1}. Young's rapidly completed predictions, with a stated accuracy of plus or minus 50 percent, are similar to our more detailed analyses, confirming that the coarse-scale ERMiT predictions are reasonable for rapid post wildfire erosion analysis. The current BAER erosion prediction technologies as utilized by Young (2016), however, do not consider the effects of roads in their analyses, which we have shown could be significant.

Comparison of Modeling Results to Observed Sediment Delivery

Following the three October, 2016 rainfall events, a large amount of sediment was produced and accumulated on the surface of road 1, in constructed detention basins along road 2, in an old quarry downhill of road 2, and on the toe slopes downhill from the fire. Vollmer (2016) reported that **227 Mg** of sediment were removed from Road 1 following the three big storm events after the wildfire. The WEPP Windows modeling based on the 22 hillslope profiles intersecting Road 1 resulted in an estimated average deposition of 40.4 kg m^{-2} (404 Mg ha^{-1} or an average depth of about 4-5 cm) on the road surface (Figs. 6 and 8). The length of Road 1 within the fire is about 790 m, and the width is about 8 m. This means the total estimated deposition is **255 Mg**, a number of similar magnitude to the amount of sediment removed.

We measured the total volume of the four sediment basins below road 2 to be 79.13 m^3. The watershed topographies describing each of the sub-catchments above these sediment basins was entered into the WEPP Windows Watershed version, and the observed dimensions of each basin, assuming an "open" or weir type outlet was described in detail in the "Structures" file in the WEPP Windows Watershed Version interface. GeoWEPP delineated the watersheds above each of the sediment basins. For the observed climate, WEPP predicted that **139.6 Mg** of sediment needed to be removed from the sediment basins following the October, 2016 storms, assuming the sediment basins were emptied when full following the storm event that filled it. The amount of sediment removed from these four basins and the downslope quarry following all three storms was estimated to be 134 m^3 (e-mail from R. Wigart, Stormwater Coordinator for the Tahoe Basin, Eldorado County, California, 13 December, 2016), which is equivalent to about **120 Mg**. Although not a formal validation, these comparisons suggest that the WEPP-predicted erosion and deposition rates following wildfire are reasonable.

Table 7. Input data for the debris flow model

Variable	Value	Units
A	51.25	Percent of basin greater than 30% steepness
R (Ruggedness)	0.528	
B	7.2	Ha; Area of moderate or high severity burn
C (Clay Content)	5.49	Percent
LL (Liquid Limit)	20	Percent
P (Total Storm Precip)		mm

Risk and volume of a Debris Flow

Table 7 presents the physical input data for the Emerald Fire derived by the WEPP Cloud interface from the USGS 30-m DEM and SSURGO database. The equations for the probability of a debris flow and the volume of a debris flow are both dependent on the storm selected. Table 8 shows the total precipitation and intensity for return periods from 1 to 200 years for storms of durations from 15 minutes to 7 days. The variables in Table 7 were combine with storms with durations from 15 minutes to 7 days, with return periods from 1 to 200 years shown in Table 8. Following the Emerald Fire, the greatest 24-h storm generated 114 mm, and the total precipitation for the three consecutive days of rain was 251 mm. These storms are approximately 10-y and 25-y recurrence interval events, and have been highlighted in Table 8.

The physical data in Table 7 were combined with the precipitation data in Table 8 in Equations 1 and 2, and the resulting probabilities of debris flow occurrence and associated volumes are presented in Table 9. The table shows that the probability of a debris flow occurring from the observed storms was around 35 percent for both the one-day and the three-day events.

Table 8. Precipitation Intensity *I* (mm h-1) and depth *P* (mm) Storm duration and frequency for the Emerald Fire location (https://hdsc.nws.noaa.gov/hdsc/pfds/). The maximum 24-h storm, a 10-y event, and 3-day rainfall depth, a 25-y event observed following the Emerald Fire are highlighted.

Recurrence Interval (years)	15-min	30-min	60-min	2-hour	3-hour	6-hour	12-hour	24-hour	2-day	3-day	4-day	7-day
2 Intensity (mm h^{-1}) Amount (mm)	33.0 (8.0)	21.0 (11.0)	15.0 (15.0)	10.0 (20.0)	8.0 (25.0)	6.0 (37.0)	5.0 (55.0)	3.0 (81.0)	2.0 (115.0)	2.0 (136.0)	2.0 (150.0)	1.0 (174.0)
5	42.0 (10.0)	27.0 (14.0)	19.0 (19.0)	13.0 (26.0)	11.0 (32.0)	8.0 (47.0)	6.0 (69.0)	4.0 (103.0)	3.0 (148.0)	2.0 (178.0)	2.0 (197.0)	1.0 (228.0)
10	50.0 (12.0)	33.0 (16.0)	22.0 (22.0)	16.0 (31.0)	13.0 (38.0)	9.0 (55.0)	7.0 (82.0)	5.0 (121.0)	4.0 (177.0)	3.0 (214.0)	2.0 (238.0)	2.0 (274.0)
25	62.0 (15.0)	40.0 (20.0)	28.0 (28.0)	19.0 (39.0)	16.0 (47.0)	11.0 (68.0)	8.0 (100.0)	6.0 (149.0)	5.0 (220.0)	4.0 (268.0)	3.0 (297.0)	2.0 (339.0)
50	72.0 (18.0)	47.0 (23.0)	32.0 (32.0)	22.0 (45.0)	18.0 (54.0)	13.0 (78.0)	10.0 (114.0)	7.0 (171.0)	5.0 (256.0)	4.0 (312.0)	4.0 (346.0)	2.0 (391.0)
100	83.0 (21.0)	54.0 (27.0)	37.0 (37.0)	26.0 (51.0)	21.0 (62.0)	15.0 (89.0)	11.0 (130.0)	8.0 (195.0)	6.0 (294.0)	5.0 (361.0)	4.0 (399.0)	3.0 (446.0)
200	96.0 (24.0)	63.0 (31.0)	43.0 (43.0)	29.0 (59.0)	24.0 (71.0)	17.0 (101.0)	12.0 (147.0)	9.0 (221.0)	7.0 (336.0)	6.0 (414.0)	5.0 (457.0)	3.0 (505.0)

Table 9. Results of debris flow estimations from Equations 1 and 2 using input data from Tables 7. For each precipitation event, the debris flow volume (m^3) is presented and the corresponding probability of occurrence (%) is in parenthesis beneath it. Cells with probabilities ≥ 50% are highlighted in red. The observed 3-day event generated 251 mm of precipitation, a 25 year event that is highlighted in yellow. The biggest 24-hr depth was 114 mm, a depth approaching a 10-year event, and the resulting debris flow risk is highlighted in blue.

Recurrence Interval (years)	**15-min**	**30-min**	**60-min**	**2-hour**	**3-hour**	**6-hour**	**12-hour**	**24-hour**	**2-day**	**3-day**	**4-day**	**7-day**
2 Volume (m^3)	533.0	579.0	647.0	743.0	820.0	1013.0	1320.0	1820.0	2569.0	3103.0	3484.0	4219.0
Probability (%)	(80.0)	(64.0)	(53.0)	(45.0)	(42.0)	(38.0)	(36.0)	(34.0)	(32.0)	(31.0)	(31.0)	(30.0)
5	575.0	631.0	716.0	838.0	936.0	1184.0	1588.0	2286.0	3441.0	4333.0	4983.0	6179.0
	(88.0)	(73.0)	(60.0)	(50.0)	(46.0)	(41.0)	(38.0)	(35.0)	(33.0)	(32.0)	(32.0)	(31.0)
10	610.0	675.0	775.0	922.0	1038.0	1336.0	1834.0	2730.0	4326.0	5625.0	6574.0	8252.0
	(93.0)	(80.0)	(66.0)	(55.0)	(50.0)	(43.0)	(39.0)	(36.0)	(34.0)	(33.0)	(32.0)	(31.0)
25	661.0	740.0	863.0	1045.0	1189.0	1565.0	2216.0	3451.0	5862.0	7950.0	9463.0	11967.0
	(97.0)	(87.0)	(74.0)	(61.0)	(55.0)	(47.0)	(42.0)	(38.0)	(36.0)	(34.0)	(33.0)	(32.0)
50	704.0	794.0	938.0	1149.0	1317.0	1762.0	2554.0	4117.0	7377.0	10328.0	12441.0	15729.0
	(98.0)	(92.0)	(79.0)	(66.0)	(59.0)	(50.0)	(44.0)	(40.0)	(37.0)	(35.0)	(34.0)	(32.0)
100	750.0	855.0	1022.0	1265.0	1460.0	1984.0	2943.0	4913.0	9297.0	13440.0	16359.0	20592.0
	(99.0)	(95.0)	(85.0)	(71.0)	(63.0)	(53.0)	(46.0)	(42.0)	(38.0)	(36.0)	(35.0)	(33.0)
200	803.0	924.0	1120.0	1397.0	1623.0	2239.0	3401.0	5884.0	11789.0	17610.0	21630.0	26981.0
	(100.0)	(97.0)	(89.0)	(76.0)	(68.0)	(57.0)f	(49.0)	(43.0)	(40.0)	(38.0)	(36.0)	(33.0)

Likelihood of a Translational Landslide

The only area of the Emerald Fire where a translational landslide would be problematic is the hillside above Highway 89 (Road 1 in Fig 1) and Cascade Road (Road 3 in Fig. 1). The dominant soil in this area is the Meeks gravelly loamy coarse sand ("30 to 70 percent slopes, extremely boulder"). The Meeks soil profile showing the depth, texture and rock content for each layer were obtained from SSURGO via WEPP Cloud[4] (Table 10). The steepness was estimated both with GeoWEPP and GIS analysis for this hillslide. The resulting properties are summarized in Table 10. The porosity of each layer, and hence its water holding capacity was estimated from the bulk density by the relationship:

$$\text{Porosity} = (1 - (\text{Bulk Density}/\text{Particle Density}) \times 100 \qquad (3)$$

The particle density was assumed to be 2.65, and the bulk density was given in the SSURGO database. The bulk density values are calculated for the soil less than 2 mm diameter. The water holding capacity can be estimated by reducing the porosity by the rock content. Hence:

[4] https://wepp1.nkn.uidaho.edu/weppcloud/

Table 10. Soil profile for Meeks gravelly loamy coarse sand

Property	Value		Units
	Layer 1	Layer 2	
Depth	330	1270	mm
Bulk Density	1.18	1.40	
Porosity	0.555	0.47	
Rock Content	28.9	90.28	percent
Maximum water holding capacity	129.3	58.2	mm
Unit water holding capacity	.3917	.0458	mm mm^{-1}

$$\text{Water Holding Capacity} = \text{Porosity} \times (1 - \text{Rock Content}) \quad (4)$$

Table 10 summarizes the soil properties important for estimating the water holding capacity of the Meeks soil. The maximum amount of water that the soil can hold is about 188 mm when the soil profile is fully saturated.

A critical input for the infinite slope equation is saturated soil thickness, D_w. As the saturated thickness increases, so does the risk of a slope failure. In order to estimate D_w, the WEPP model was run for 100 years, and the cumulative distribution of soil water content plotted (Fig. 9). The saturated soil thickness can be determined from the soil water content D_w by the relationship:

$$D_w = \text{Water Content/Unit Water Holding Capacity} \quad (5)$$

From the cumulative distribution of soil water content shown in Fig. 9 and equation 5, it was possible to determine the probability of exceeding a value for D_w.

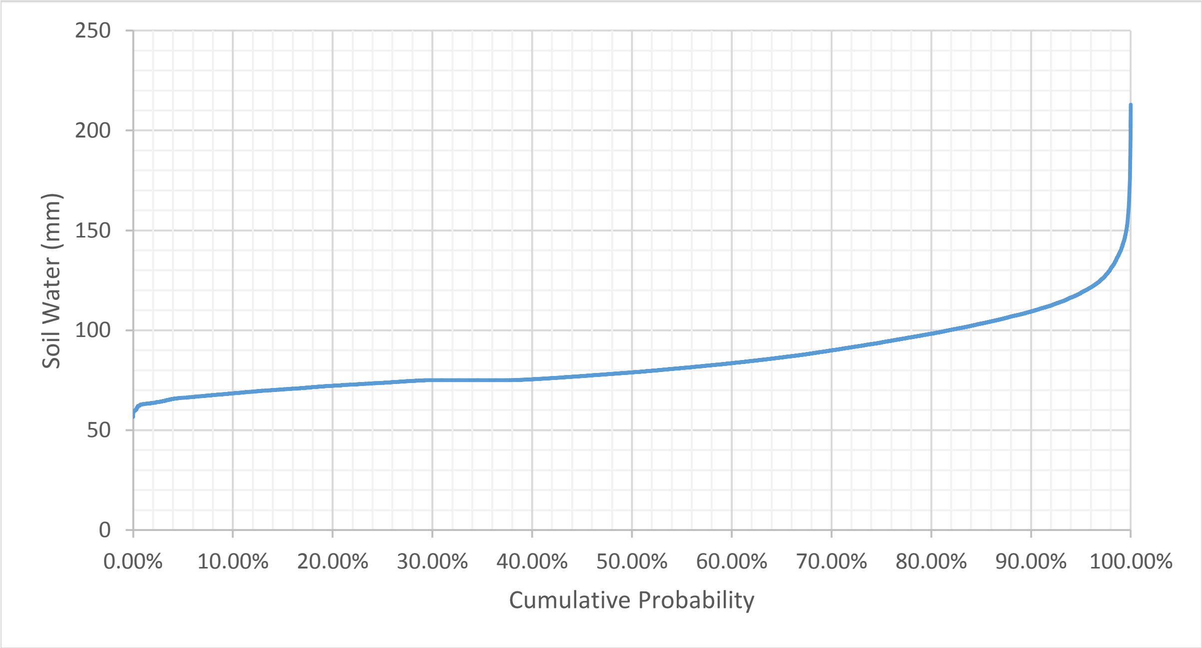

Fig. 9. Soil water content as predicted from a 100-years WEPP run versus cumulative probability.

Table 11. Soil strength properties for the Meeks soil for the infinite slope equation

Variable	Value	Units
Soil Cohesion *C'*	0	PSF (Pounds per square foot)
Slope Steepness α	25	Degrees
Tree Surcharge q_0	15 or 0	PSF
Root strength C_r	100 or 0	PSF
Moist Soil Specfic Weight γ	110	PCF (Pounds per cubic foot)
Soil Thickness *D*	5.25	Ft
Saturation Thickness *Dw*	4.167 – 5.25	Ft
Saturated Specific Weight γ_{sat}	115.22	PCF
Dry Soil Specific Weight γ_d	73.75	PCF
Water Specific Weight γ_w	62.5	PCF
Soil Internal Friction Angle ϕ'	35	Degrees

For applying the infinite slope equation, to minimize the risk of conversion errors, all calculations were done in English units as shown in Equation 3. Estimates for the input values were obtained from Hammond et al. (1992) who provide a large database of inputs for the infinite slope model. The assigned values are summarized in Table 11. The Factor of Safety *FS* was then determined for the prefire condition with tree surcharge and tree root strength, and for four to six years postfire with no tree surcharge, for different amounts of soil water. The results of the analysis are presented in Table 12 along with the probabilities for each saturated thickness of soil. Table 12 shows that in the prefire condition, the Factor of Safety was greater than 1.0 for all values of D_w, the saturated soil depth, and hence the slope was stable even when fully saturated. However, in four to six years following the fire, when the roots from the dead trees have decayed and the mass of the above ground live biomass surcharge is reduced through tree decay, there is a high likelihood that the slope above Highway 89 will become unstable even for moderate depths of saturated soil. Table 12 shows that there is nearly a 100 percent probability that D_w will exceed 4 ft, and at that depth of soil water, the Factor of Safety becomes less than 1, suggesting that there is a high likelihood of a translational landslide.

Table 12. Probability of a given depth of soil water D_w and Factor of safety for different depths of soil water before and four to six years after a wildfire

D_w (ft)	$P(D_w)$	Before Fire FS	After Fire FS
1	1	1.781382	1.34054
1.5	1	1.702	1.26109
2	1	1.623306	1.18235
3	1	1.467943	1.02694
4	1	1.315225	0.87424
4.5	0.1823	1.239837	0.79888
5	0.002	1.165084	0.72418

Deposition from Dry Ravel

The dry ravel analysis was completed by the Michigan Technological Research Institute using an online tool they have developed for the Fu (2004) model they name Ravel Rat[5]. The Emerald Fire soil burn severity map was formatted as a 30-m raster file, and uploaded into the Ravel Rat online interface. The model was run, and identified the cells of deposition. Ravel Rat offers several output formats including an *.mxd file for viewing results in a GIS and a *.kml file for viewing in Google Earth. Figure 10 shows the predicted zones of dry ravel deposition as a screen capture from Google Earth. Most of the depositional cells are within the burned site, but several cells are on highway 89.

4. Discussion

Road segment effect on surface flow pattern and soil loss

In the absence of fire, upslope runoff and sediment delivery to Road 1 is minimal. The results in Table 3 and Fig. 4 show that after the fire, road segments intercepted upstream runoff and were sites of sediment

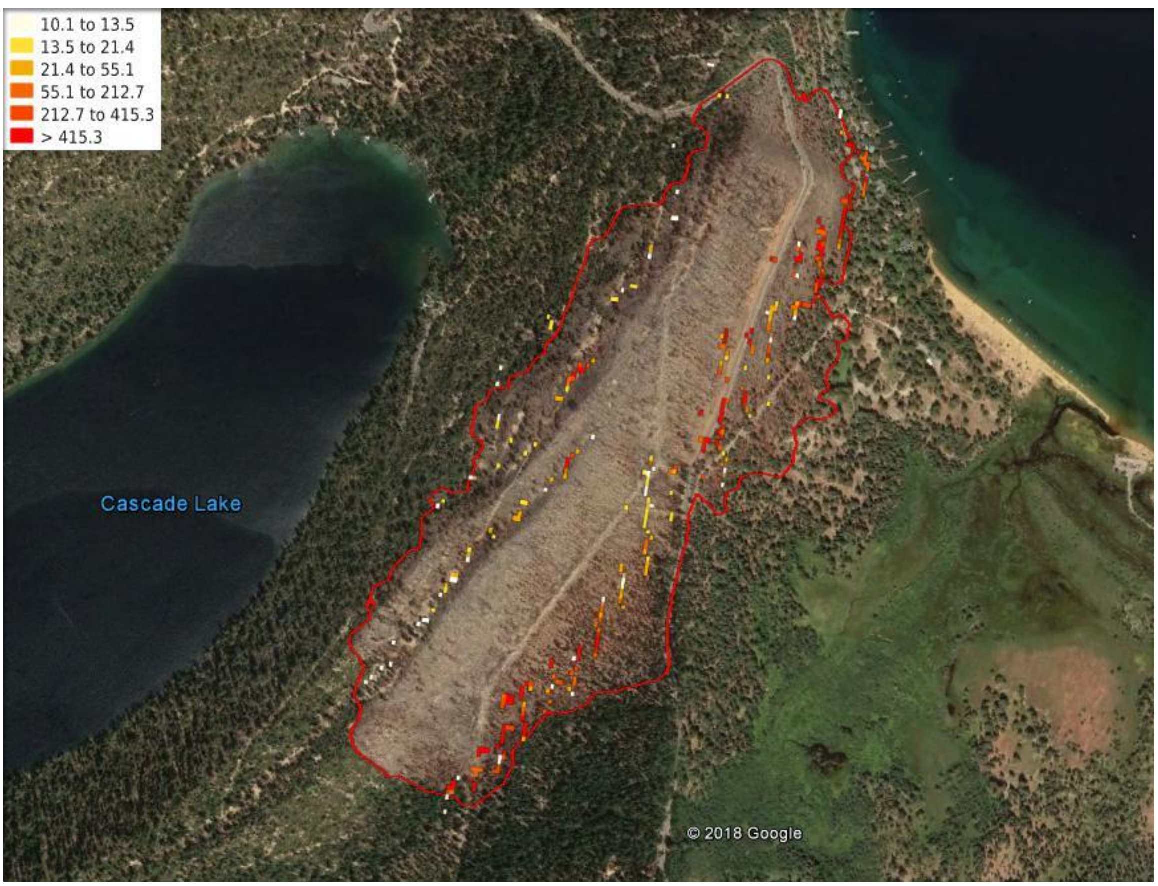

Figure 10. Screen capture of Google Earth image the distribution of cells with predicted sediment deposition from dry ravel following the Emerald Fire.

[5] http://spatial.mtri.org/ravelrat/calculator

deposition. Generally, sediment deposition is likely on a low gradient road surface, as the much lower slope greatly reduces sediment transport capacity (Finkner et al., 1989; Gucinski et al., 2001; MacDonald and Coe, 2008). The estimated deposition is evident in the road-related yellow deposition pixels shown in Fig. 6 and in the negative soil loss, indicating a location of deposition, in Fig. 8. With the large amount of postfire sediment deposition and clear water accumulation on a paved road surface, the increased flow from roads has a relatively low sediment concentration and therefore can detach more soil particles (Finkner et al., 1989). This may partially explain the high onsite soil loss rate within short distances below road segments in Fig. 7 (b, c) and the spike in soil loss after deposition in Fig. 8. On the other hand, the reduced number of flow paths which leave roads (Table 3) implies some runoff accumulation and relatively smaller areas below road segments are more likely to be scoured by the increased uphill flow.

In the case of continuous upstream runoff accumulation along natural hillslopes, discharge is assumed to increase linearly and thus flow shear stress can be expressed as a function of downslope distance (Finkner et al., 1989). This explains the increasing soil loss rate from ridge (Fig. 7a) and before the deposition on road surface (Fig. 8).

The road segments within the burnt area are typical cut-and-fill roads in which the excavated material uphill of the road centerline is placed downhill of the centerline and forms an oversteepened fillslope. The gradient of fillslope is greater than the original topography as the extra material increases the elevation difference. This is another clue to explain the high onsite soil loss rate within the 10 m buffer belt below the road segment (Fig. 7 b and c) and the sharp soil loss increase after leaving road in Fig. 8. Further downhill, the slope decreases as does the predicted erosion rate, until ultimately, deposition begins to occur.

Figures 4, 5 and 6 all show different ways of seeing how a road can alter the boundary of sub-catchments and hydrological units on a postfire landscape. Table 4 and Fig. 4 show that a road segment can act as a boundary between sub-catchments, and in some cases, forming new sub catchments downhill from a road (Figure 5). The new sub catchments below roads tend to have shorter flow paths, and hence, are at less risk to concentrated flow erosion (Table 5). On the other hand, the flow length accumulation along roads in Fig. 5 shows that road segments can also function as flow diverters, transporting sediment from one sub-catchment to a nearby sub-catchment. Road 2 is a good example of flow diversion as it has been identified as a channel in Fig. 3, increasing the runoff and sediment yield from the adjacent subwatershed.

The importance of road design

Our results show the importance of the road drainage system in a postfire watershed in altering surface hydrologic and soil loss processes. A field survey confirmed the LIDAR topography with road 1 flat and lacking culverts or an inside drainage ditch within the eastern part of the burnt area. Much of the upslope runoff either followed or crossed over the road surface, depositing sediment as it passed. Conversely, there were several ditches defined by the LIDAR DEM and verified by our field visit along road 2. Road-intercepted runoff was channeled along the ditches to culverts and downhill sediment basins rather than flooding over the road surface. Therefore the land surface below road 2 was not impacted by upslope runoff and the erosion risk was limited to channels which tended to be more armored than the burned hillslope (Fig. 3). The upslope ditches and regularly spaced culverts on road 2 demonstrate the potential for road networks to reduce erosion risks in forests following wildfire.

The effect of fire disturbance

Generally, the net effect of a road network in a forest has been reported to increase basin wide sediment production (Wemple et al., 2001). When forests are disturbed by fire as in this study, surface runoff and soil erosion are greatly increased. This means more flow paths will be generated under similar rainfall as compared to the pre-fire conditions. As shown in Table 3, a larger portion of upstream flow paths were stopped by road segments when intercepting the dense inflow than when intercepting the sparse ones. This implies roads will be relatively more efficient in altering surface flow patterns under the postfire conditions. Road segments that intercept upstream runoff may prevent sediment from being transported to downstream channels. From this perspective, a road can act as a hydrologic barrier and be helpful in reducing sediment yield in a fire disturbed forest (Gucinski et al., 2001).

On the other hand, roads can transport the high sediment loads that result from surface erosion. Sediment and other debris can accumulate and block ditches and culverts, leading to road damage and failures that compound the erosion (Foltz et al., 2009). The detailed WEPP results for Fig. 3 showed high sediment yield near channel outlets below the road. In the one watershed that included the Road 1 culvert near the junctions of Roads 1 and 2, channel erosion was predicted to be the source of 20 percent of the total sediment delivered from this watershed. Sediment basins, channel energy dissipation structures and in-channel grade control structures (Napper, 2006) may be beneficial to control erosion on such steep channels and to reduce the risk of gully initiation.

Risk of Debris Flows

Overall the predicted risk of a debris flow occurring was only 35% (Table 9). This low value is due in part to the relatively small area of the fire, and hence the small areas of steep land and burned land that are inputs to the model (Equations 1 and 2). There is only one major channel within the fire perimeter, and during a field visit following the fire, there was no evidence that any mass movement had occurred in this channel.

The Risk of a Translational Landslide

The results of the infinite slope equation indicate that before the fire, the slope was stable, regardless of the depth of soil water. Following the fire, however, there is a high probability that a landslide could occur. The large retaining wall along the side of the road suggests that there were concerns in the past about this type mass failure in the past. The presence of the retaining wall may be adequate to prevent the initiation of a translational landslide in the future.

The risk of Dry Ravel

If dry ravel was going to occur, it is likely to be widely dispersed over the fire area, with only a minimal amount of deposition predicted for Highway 89, and even less for Cascade Road (Figure 10). Dry ravel was only a concern for late summers in 2017 and 2018 if the soils became sufficiently dry to lose their hygroscopic forces holding loose particles in place. Shrub regrowth will stabilize loose soil on the hillslope in the future. The authors are not aware of any dry ravel events the past two summers.

Conclusions

Through a GIS-based soil erosion model and high resolution LiDAR terrain data, this study provided a spatial analysis of road-related flow path delineation and soil loss in postfire forest conditions. Fire disturbance greatly increased the soil erosion risk within the fire boundary to estimated levels greater than 4 Mg ha^{-1} yr^{-1} for nearly 80% of the burnt area. Our model predictions were not very different from reported sediment deposition immediately following the fire. The modelling showed that even though roads are generally thought to exacerbate erosion problems, in the postfire environment they had complex and variable effects on runoff and sediment transport. Overall the roads and downstream system of detention basins created opportunities to catch a considerable amount of sediment. In some cases, the roads diverted upland runoff and sediment to the adjacent subwatershed. The road fillslopes were predicted to be at risk for high onsite soil loss risk, as were channels downstream of roads. The modeling and onsite observations suggest that a properly designed road drain system, including well-spaced culverts with energy dissipating outlets, can reduce the likelihood of water and sediment flooding over the road surface and minimize the risk of downstream channel erosion or gullying. The risks of a debris flow following the fire were low. Minimal deposition on the roads due to dry ravel was predicted. Our results suggest that there is a risk of a translational slope failure on the slopes above Highway 89 during the late winter or early spring of 2020-2022, depending on winter soil water conditions, although a retaining wall along the road may mitigate that hazard.

ACKNOWLEDGEMENTS

This study was supported by the USDA Forest Service Pacific Southwest Research Station, using funds provided by the Bureau of Land Management through the sale of public lands as authorized by the Southern Nevada Public Land Management Act. The study was also supported by the China Scholarship Council (Project 201604910077), the National Natural Science Foundation of China (Project 41571273) and Natural Science Foundation of Jiangsu Province, China (Project BK2015610).

References

Akay AE, Erdas O, Reis M, Yuksel A (2008) Estimating sediment yield from a forest road network by using a sediment prediction model and GIS techniques. *Building and Environment* **43**, 687–695. doi:10.1016/j.buildenv.2007.01.047.

Araujo HA, Page A, Cooper AB, Venditti J, MacIsaac E, Hassan MA, Knowler D (2014) Modelling changes in suspended sediment from forest road surfaces in a coastal watershed of British Columbia. *Hydrological Processes* **28**, 4914–4927. doi:10.1002/hyp.9989.

Brooks ES, Boll J, Elliot WJ, Dechert T (2006) Global Positioning System/GIS-based approach for modeling erosion from large road networks. *Journal of Hydrologic Engineering* **11**, 418–426. doi:10.1061/(ASCE)1084-0699(2006)11:5(418).

Brooks ES, Dobre M, Elliot WJ, Wu JQ, Boll J (2016) Watershed-scale evaluation of the Water Erosion Prediction Project (WEPP) model in the Lake Tahoe basin. *Journal of Hydrology* **533**, 389–402. doi:10.1016/j.jhydrol.2015.12.004.

Cannon SH, , Gartner JE, Rupert MG, Michael JA, Rea AH, Parrett C (2010) Predicting the probability and volume of postwildfire debris flows in the intermountain western United States. *GSA Bulletin* January/February 122(1/2):127-144.

Croke J, Mockler S (2001) Gully initiation and road-to-stream linkage in a forested catchment, southeastern Australia. *Earth Surface Processes and Landforms* **26**, 205–217. doi:10.1002/1096-9837(200102)26:2<205::AID-

ESP168>3.0.CO;2-G.

Coats R, Larsen M, Heyvaert A, Thomas J, Luck M, Reuter J (2008) Nutrient and sediment production, watershed characteristics, and land use in the Tahoe Basin, California-Nevada. *Journal of the American Water Resources Association* **44**, 754–770. doi:10.1111/j.1752-1688.2008.00203.x.

DeBano LF, Neary D, Ffolliott P (1998) Fire's effects on ecosystems. John Wiley & Sons: New York.

Elliot WJ (2004) WEPP Internet interfaces for forest erosion prediction. *Journal of the American Water Resources Association* **40**, 299–309. doi:10.1111/j.1752-1688.2004.tb01030.x.

Elliot WJ (2013) Erosion processes and prediction with WEPP technology in forests in the Northwestern U.S. *Transactions of the ASABE* **56**, 563–579. doi:10.13031/2013.42680.

Elliot WJ, Hall DE (2010) Disturbed WEPP Model 2.0. Ver. 2014.04.14. Moscow, ID: U.S. Department of Agriculture, Forest Service, Rocky Mountain Research Station. Online at < https://forest.moscowfsl.wsu.edu/fswepp/ >.

Elliot WJ, Miller ME, Enstice N (2016) Targeting forest management through fire and erosion modelling. *International Journal of Wildland Fire* (25): 876-887. doi: 10.1071/WF15007 .

Elliot WJ, Robichaud PR (2001) Comparing erosion risks from forest operations to wildfire. In: Procs of The International Mountain Logging and 11th Pacific Northwest Skyline Symposium. University of Washington, Seattle, WA.

Flanagan DC, Nearing MA (eds.) (1995) *USDA-Water Erosion Prediction Project (WEPP) Hillslope Profile and Watershed Model Documentation*. NSERL Report No. 10, National Soil Erosion Research Laboratory, USDA-Agricultural Research Service, West Lafayette, Indiana. 285 p.

Flanagan DC, Frankenberger JR, Cochrane TA, Renschler CS, Elliot WJ (2013) Geospatial application of the Water Erosion Prediction Project (WEPP) model. *Transactions of the ASABE* **56**, 591–601. doi:10.13031/2013.42681.

Finkner SC, Nearing MA, Foster GR, Gilley JE (1989) A simplified equation for modeling sediment transport capacity. *Transactions of the ASAE* **32**, 1545–1550. doi:10.13031/2013.31187.

Foltz RB, Robichaud PR, Rhee H (2009) A synthesis of post-fire road treatments for BAER teams: methods, treatment effectiveness, and decision making tools for rehabilitation. Gen. Tech. Rep. RMRS-GTR-228. Fort Collins, CO: U.S. Department of Agriculture, Forest Service, Rocky Mountain Research Station. 152 p.

Fu, X (2004) A physical model of dry ravel. MS Thesis. Pullman, WA: Washington State University. 114 p.

Grace, III, JM (2017) Predicting forest road surface erosion and storm runoff from high-elevation sites. *Transactions of the ASABE* 60(3):705-719. https://doi.org/10.13031/trans.11646.

Gucinski H, Furniss MJ, Ziemer RR, Brookes MH (2001) Forest roads: a synthesis of scientific information. Gen. Tech. Rep. PNWGTR-509. Portland, OR: U.S. Department of Agriculture, Forest Service, Pacific Northwest Research Station. 103 p.

Hammond, C, Hall, D, Miller, S, Swetik, P (1992) Level I Stability Analysis (LISA) Documentation for Version 2.0. Ogden, UT: U.S.D.A. Forest Service, Intermountain Research Station, General Technical Report INT-285, 190p.

Helsel, DR, Hirsch RM (2002) Statistical Methods in Water Resources: U.S. Geological Survey Techniques of Water Resources Investigations, Book 4, Chapter A3, 510 p., http://pubs.usgs.gov/twri/twri4a3/html/pdf new.html (August 2005).

Jones JA, Grant GE (1996) Peak flow responses to clear-cutting and roads in small and large basins, western Cascades, Oregon. *Water Resources Research* **32**, 959–974. doi:10.1029/95WR03493.

Katz HA, Daniels JM, Ryan S (2014) Slope-area thresholds of road-induced gully erosion and consequent hillslope-channel interactions. *Earth Surface Processes and Landforms* **39**, 285–295. doi:10.1002/esp.3443.

Laflen JM, Elliot WJ, Flanagan DC, Meyer CR, Nearing MA (1997) WEPP–Predicting water erosion using a process-based model. *Journal of Soil and Water Conservation* **52**(2), 96-102.

MacDonald LH, Coe DBR (2008) Road sediment production and delivery: processes and management. In: Proceedings of the First World Landslide Forum, International Programme on Landslides and International Strategy for Disaster Reduction. United Nations University, Tokyo, Japan, pp. 381–384.

McCormick FH, Riemen BE, Kershner JL (2010) Biological responses to stressors in aquatic ecosystems in Western North America: Cumulative watershed effects of fuel treatments, wildfire, and post-wildfire remediation. Chapter 11. IN Elliot, WJ, Miller IS, and Audin L. eds. *Cumulative Watershed Effects of Fuel Management in the Western United States*. Gen. Tech. Rep. RMRS-GTR-231. Fort Collins, CO: U.S. Department of Agriculture, Forest Service, Rocky Mountain Research Station. 206-233.

Melton, MA (1965) The geomorphic and paleoclimatic significance of alluvial deposits in southern Arizona: *The Journal of Geology* (73): 1–38.

Miller ME, Billmire M, Banach D (2015) NASA BAER user manual for running GeoWEPP. Online at: <http://geodjango.mtri.org/geowepp/ >

Miller ME, Elliot WJ, Billmire M, Robichaud PR, Endsley KA (2016) Rapid response tools and datasets for post-fire remediation: Linking remote sensing and process-based hydrologic models. *International Journal of Wildland Fire* **25**, 1061–1073. doi:10.1071/WF15162.

Napper, C (2006) Burned area emergency response treatments catalog. 0625 1801-SDTDC. San Dimas, CA: USDA Forest Service, Sand Dimas Technology and Development Center. 266 p.

Nevada Division of Environmental Protection (2011) Final Lake Tahoe Total Maximum Daily Load. Online at < *https://www3.epa.gov/region9/water/tmdl/laketahoe/final-lake-tahoe-tmdl.pdf* >, Carson City, NV.

Parsakhoo A, Lotfalian M, Kavian A, Hosseini SA (2014) Prediction of the soil erosion in a forest and sediment yield from road network through GIS and SEDMODL. *International Journal of Sediment Research* **29**, 118–125. doi:10.1016/S1001-6279(14)60027-5.

Parsons A, Robichaud PR, Lewis SA, Napper C, Clark JT (2010) Field guide for mapping post-fire soil burn severity, General Technical Report RMRS-GTR-243. Fort Collins, CO: Rocky Mountain Research Station. 49 p.

Persendt FC, Gomez C (2016) Assessment of drainage network extractions in a low-relief area of the Cuvelai Basin (Namibia) from multiple sources: LiDAR, topographic maps, and digital aerial orthophotographs. *Geomorphology* **260**, 32–50. doi:10.1016/j.geomorph.2015.06.047.

Reid, LM (2010) Cumulative effects of fuel treatments on channel erosion and mass wasting, Chapter 10. IN Elliot, WJ, Miller IS, and Audin L. eds. *Cumulative Watershed Effects of Fuel Management in the Western United States*. Gen. Tech. Rep. RMRS-GTR-231. Fort Collins, CO: U.S. Department of Agriculture, Forest Service, Rocky Mountain Research Station. 101-125.

Robichaud PR (2005) Measurement of post-fire hillslope erosion to evaluate and model rehabilitation treatment effectiveness and recovery. *International Journal of Wildland Fire* **14**, 475–485. doi: 10.1071/WF05031.

Robichaud PR, Beyers JL, Neary DG (2000) Evaluating the effectiveness of postfire rehabilitation treatments, Gen. Tech. Rep. RMRS-GTR-63, Fort Collins, CO: U.S. Department of Agriculture, Forest Service, Rocky Mountain

Research Station. 85p.

Robichaud PR, Elliot WJ, Pierson FB, Hall DE, Moffet CA (2007) Predicting postfire erosion and mitigation effectiveness with a web-based probabilistic erosion model. *Catena* **71**, 229–241. doi:10.1016/j.catena.2007.03.003.

Robichaud PR, Wagenbrenner JW, Brown RE (2010) Rill erosion in natural and disturbed forests: 1. Measurements. *Water Resources Research* **46**, W10506. doi:10.1029/2009WR008314.

Sosa-Pérez G, MacDonald LH (2017) Wildfire effects on road surface erosion, deposition, and road–stream connectivity. *Earth Surface Processes and Landforms* **42**, 735–748. doi:10.1002/esp.4018

Soulis KX, Dercas N, Papadaki CH (2015) Effects of forest roads on the hydrological response of a small-scale mountain watershed in Greece. *Hydrological Processes* **29**, 1772–1782.doi:10.1002/hyp.10301.

Staley DM, Negri DA, Kean JW, Laber HM, Tillery AC, Yougerg AM (2016) Updated logistic regression equations for the calculation of post-fire debris-flow likelihood in the Western United States, USGS Open-File Report 2016-1106. Reston, VA: U.S. Geological Survey. 17 p.

Thomaz EL, Vestena LR, Ramos Scharrón CE (2014) The effects of unpaved roads on suspended sediment concentration at varying spatial scales – a case study from Southern Brazil. *Water and Environment Journal* **28**, 547–555. doi:10.1111/wej.12070.

United States Geological Survey (USGS) (2018) USGS Geologists Study Debris-Flow Aftermath in Montecito. Online at < https://www.usgs.gov/news/usgs-geologists-join-efforts-montecito-assess-debris-flow-aftermath >

Vollmer M (2016) Emerald fire update. Presentation to Tahoe Regional Planning Authority Advisory Planning Commission on 8 November, 2016.

Wemple BC, Swanson FJ, Jones JA (2001) Forest roads and geomorphic process interactions, Cascade Range, Oregon, *Earth Surfaces Processes and Landforms* **26**, 191–204. doi:10.1002/1096-9837(200102)26:2<191::AID-ESP175>3.0.CO;2-U.

Wemple BC, Jones JA, Grant GE (1996) Channel network extension by logging roads in two basins, western Cascades, Oregon. *Water Resources Bulletin* **32**, 1195–1207. doi:10.1111/j.1752-1688.1996.tb03490.x.

Wemple BC, Clark GE, Ross DS, Rizzo DM (2017) Identifying the spatial pattern and importance of hydro-geomorphic drainage impairments on unpaved roads in the northeastern USA. *Earth Surfaces Processes and Landforms* **42**, 1652–1665. doi:10.1002/esp.4113.

Yang P, Ames DP, Fonseca A, Anderson D, Shrestha R, Glenn NF, Cao Y (2014) What is the effect of LiDAR-derived DEM resolution on large-scale watershed model results? *Environmental Modelling & Software* **58**, 48–57. doi:10.1016/j.envsoft.2014.04.005.

Young D (2016) BAER assessment soils report – Emerald Fire. Redding, CA: U.S. Department of Agriculture, Forest Service, Region 5, Shasta-Trinity National Forest. 13 p.